Meson-exchange currents and quasielastic predictions for charged-current neutrino-^{12}C scattering in the superscaling approach

G. D. Megias,[1,*] T. W. Donnelly,[2] O. Moreno,[2] C. F. Williamson,[2] J. A. Caballero,[1] R. González-Jiménez,[1] A. De Pace,[3] M. B. Barbaro,[4,3] W. M. Alberico,[4,3] M. Nardi,[3] and J. E. Amaro[5]

[1]*Departamento de Física Atómica, Molecular y Nuclear, Universidad de Sevilla, 41080 Sevilla, Spain*
[2]*Center for Theoretical Physics, Laboratory for Nuclear Science and Department of Physics,*
Massachusetts Institute of Technology, Cambridge, Massachusetts 02139, USA
[3]*Istituto Nazionale di Fisica Nucleare, Sezione di Torino, Via Pietro Giuria 1, 10125 Torino, Italy*
[4]*Dipartimento di Fisica, Università di Torino, Sezione di Torino, Via Pietro Giuria 1, 10125 Torino, Italy*
[5]*Departamento de Física Atómica, Molecular y Nuclear*
and Instituto Carlos I de Física Teórica y Computacional,
Universidad de Granada, 18071 Granada, Spain

We evaluate and discuss the impact of meson-exchange currents (MECs) on charged-current quasielastic neutrino cross sections. We consider the nuclear transverse response arising from two-particle two-hole states excited by the action of electromagnetic, purely isovector meson-exchange currents in a fully relativistic framework based on the work by the Torino Collaboration [A. D. Pace, M. Nardi, W. M. Alberico, T. W. Donnelly, and A. Molinari, Nucl. Phys. A726, 303 (2003)]. An accurate parametrization of this MEC response as a function of the momentum and energy transfers involved is presented. Results of neutrino-nucleus cross sections using this MEC parametrization together with a recent scaling approach for the one-particle one-hole contributions (named SuSAv2) are compared with experimental data.

I. INTRODUCTION

A correct interpretation of atmospheric and accelerator-based neutrino oscillation experiments strongly relies on our understanding of neutrino-nucleus scattering at inter-mediate energies (from 0.5 to 10 GeV) and in particular of the nuclear-structure effects involved. One of the simplest descriptions of the nucleus, the relativistic Fermi gas (RFG) model, which is known to be inadequate for inclusive electron scattering in the quasielastic (QE) regime [1], also fails to reproduce recent measurements of QE neutrino and antineutrino scattering cross sections [2–7]. This supports the need for considering mechanisms such as final-state interactions, nuclear correlations, or meson-exchange currents (MECs), in particular through their contribution to multinucleon knockout around and beyond the QE peak as suggested by explicit modeling [8–10].

In particular, the recent muon neutrino charged-current quasielastic (CCQE) cross sections measured by the MiniBooNE Collaboration [2,3] show discrepancies with a RFG description of the nuclear target. This simple model, widely used in experimental analyses, underestimates the total cross section, unless *ad hoc* assumptions are made such as a larger mass parameter in the nucleon axial form factor ($M_A = 1.35$ GeV/c^2 versus $M_A = 1.032$ GeV/c^2). Relativistic effects cannot be neglected for the kinematics

of experiments such as MiniBooNE, with neutrino energies as high as 3 GeV. Although the RFG model has the merit of accounting properly for relativistic effects, it is too crude to account for detailed nuclear dynamics, as is well known from comparisons with QE electron scattering data [11]. More sophisticated relativistic nuclear models have been applied in recent years to neutrino reactions. In addition, phenomenological techniques have been proposed, such as the superscaling approach (SuSA) [12] which assumes the existence of universal scaling functions for the electromagnetic and weak interactions. Analyses of inclusive (e, e') data have shown that at energy transfers below the QE peak, superscaling is fulfilled rather well [13–15], which implies that the reduced cross section is largely independent of the momentum transfer (first-kind scaling) and of the nuclear target (second-kind scaling) when expressed as a function of the appropriate scaling variable. From these analyses, a phenomenological scaling function was extracted from the longitudinal QE electron scattering responses. It was subsequently used to predict neutrino-nucleus cross sections by multiplying it by the single-nucleon weak cross sections, assuming that the single universal scaling function was appropriate for all of the various responses involved, namely, CC, CL, LL, T(VV), T(AA), and T′(VA). In this work, we will use a recently developed improved version of the superscaling model called SuSAv2 [16] that incorporates relativistic mean field (RMF) effects [17–19] in the longitudinal and transverse nuclear responses, as well as in the isovector and isoscalar

*Corresponding author.
megias@us.es

channels independently. Three reference scaling functions are provided to describe in a consistent way both electron- and (anti)neutrino-nucleus reactions in the QE region: transverse ($\tilde{f}_T$), longitudinal isovector ($\tilde{f}_L^{T=1}$), and longitudinal isoscalar ($\tilde{f}_L^{T=0}$). This model also includes in a natural way an enhancement of the transverse response through RMF effects without resorting to inelastic processes or two-particle emission via MECs.

Strictly speaking, only the longitudinal part of the response appears to superscale; in the scaling region, some degree of scaling violation is found which can be attributed to the transverse part of the response. The assumption that the various types of responses [CC, CL, LL, T(VV), T(AA) and T′(VA)] scale the same way has been denoted as zeroth-kind scaling; the most recent SuSAv2 approach builds in the degree of violation of zeroth-kind scaling demanded by the RMF results. Specifically, the longitudinal contributions, apparently being essentially impulsive at high energies, are usually used to determine the basic nuclear physics of QE scattering, notably, including any correlations present in that sector, since the results are obtained by fitting electron scattering data. Beyond the QE region, it is natural to have scaling violations, since the reaction mechanism there is not solely the impulsive knockout of a nucleon but may proceed via meson production including baryon resonances such as the Δ. It is known that the latter contributions are much more prominent in the transverse than in the longitudinal responses [12,20]. However, it is also known that even with only the one-particle one-hole (1p-1h) contributions there are expected to be violations of zeroth-kind scaling arising from purely dynamical relativistic effects (see the discussions of how the SuSAv2 approach is constructed).

However, even below the meson production threshold, there are scaling violations in the transverse response [15], one source of which could be the MEC contributions, again predominantly transverse. The MECs are two-body currents that can excite both 1p-1h and two-particle two-hole (2p-2h) states. Most studies of electromagnetic (e, e') processes performed for low-to-intermediate momentum transfers with MECs in the 1p-1h sector (see, e.g., [21–24]) have shown a small reduction of the total response at the QE peak, mainly due to diagrams involving the electro-excitation of the Δ resonance; they are roughly compensated by the positive contributions of correlation diagrams, where the virtual photon couples to a correlated pair of nucleons. In the present work, we shall, therefore, neglect them and restrict our attention to 2p-2h final states computed in a fully relativistic way. It has been found [8–10,25,26] that the MECs give a significant positive contribution to the cross section, which helps to account for the discrepancy observed in (e, e') processes between theory and experiment in the "dip" region between the QE peak and Δ resonance as well as for the discrepancies between some recent neutrino CCQE measurements (e.g.,

MiniBooNE, NOMAD, and MINERνA). In particular, in [27,28], we used a parametrization of the results of [29] to evaluate the contribution of MECs to the vector transverse (anti)neutrino response at MiniBooNE kinematics.

The presence of nucleon-nucleon correlation interactions involving the one-nucleon current may lead to the excitation of 2p-2h final states, and interference between these processes and those involving MECs must also be taken into account. The results of calculations carried out within the Green's function Monte Carlo approach [30] suggest that these interference contributions may, in fact, be quite large. This is in agreement with our preliminary calculation of the correlation current plus MEC effects in the response functions within the scheme of the relativistic Fermi gas model [31]. These effects, also taken into account in the RFG-based descriptions of 2p-2h provided by Martini *et al.* [8] and Nieves *et al.* [9], are not included explicitly in our RFG MEC model that relies on a hybrid description where the one-particle emission already contains contributions of nuclear ejections due to nuclear correlations—through the experimental scaling function. Explicit calculations of the correlation-MEC interference terms are still in progress, and their contributions will be presented in a forthcoming publication.

This paper is organized as follows. In Sec. II we briefly describe the computation of the MECs considered in this work and show for the first time the corresponding responses of ^{12}C for several momentum transfers as a function of the QE scaling variable. We also show a new parametrization of these responses and compare it with the one used in [10,27,28]. In Sec. III we apply the new MEC parametrization and the SuSAv2 model to the computation of neutrino-^{12}C CCQE cross sections and compare the results with MiniBooNE, NOMAD, and MINERνA data. Finally, in Sec. IV we show the conclusions of our analysis.

II. RESULTS FOR MEC RESPONSES

We consider in this work the purely isovector pion-exchange currents involving virtual Δ resonances as well as the seagull (contact) and pion-in-flight currents obtained in previous work [29,32]. The evaluation was performed within the RFG model in which a fully Lorentz and transitionally invariant calculation of the MEC can be developed. Deviations from the Fermi gas model 2p-2h responses produced by ingredients such as final-state interactions, finite nuclear effects, or nuclear correlations are expected to be moderate, which would result in small corrections in the impulsive cross section as the MEC contributions are also moderate.

The previous statement is not insubstantial, and it requires further explanation. We expect the finite-size effects to be moderate on the 2p-2h responses. This is in accordance with the calculations performed by one of the authors and presented in a series of papers (see, for instance, [33,34]). These are the only calculations up to

date concerning the inclusive 2p-2h transverse response function at low-to-intermediate momentum transfers for ^{12}C and ^{40}Ca within the framework of the continuum shell model. The results were similar to those found in nuclear matter by Van Orden and Donnelly [35], Alberico et al. [36], and Dekker et al. [37]. The nonrelativistic 2p-2h response function is a rather smooth function. Its general behavior is clearly dominated by the 2p-phase space and by the nucleon and pion electromagnetic form factors, whereas it is rather insensitive to details of the finite-size nucleus.

The previous works together with [29,38] are the only calculations available for the 2p-2h electromagnetic responses for medium nuclei. The studies presented in [29,37] clearly showed that the relativistic effects, mainly in the delta MEC, dominate the 2p-2h transverse response.

It has been known for a long time that ground-state correlations deplete the occupation numbers of the hole states, the values of which drop from unity to ~0.8. The main effect of such depletion is known to be a redistribution of the strength to higher energies. In the case of the longitudinal response dominated by the impulse approximation, this is translated into a hardening of the response function with respect to an uncorrelated model, like the Fermi gas or the semirelativistic shell model [39], with the appearance of a long tail at high energy. This is precisely the shape of the scaling function we are using. Being a phenomenological observable, the scaling function already contains all the physics embodied in the nuclear-structure details, including correlations, depletions, and final-state interactions.

In the case of the 2p-2h contributions, one expects the depletion of the occupation numbers also to produce a redistribution of the strength to higher energies. Although this could modify the position of the peak in the 2p-2h response function, the resulting redistribution is expected to keep some resemblance with the behavior already shown in the 1p-1h channel.

As mentioned above, the kinematical regions contained under the integral over the neutrino fluxes considered here extend to relativistic domains so that a relativistic treatment of the process is required. As was discussed in the previous work [29,32], relativistic effects are important to describe the nuclear transverse response function for momentum transfers above 500 MeV/c.

All possible 2p-2h many-body diagrams containing two pionic lines and the virtual boson attached to the pion (pion-in-flight term), to the $NN\pi$ vertex (seagull or contact term), or involving the virtual Δ resonance are taken into account to compute the vector-vector transverse MEC response, $R_{T,\text{VV}}^{\text{MEC}}$, of ^{12}C [29]. These responses can be given as a function of the energy transfer ω' or of the scaling variable Ψ' related through

$$\Psi' = \frac{1}{\sqrt{\xi_F}} \frac{\lambda' - \tau'}{\sqrt{(1+\lambda')\tau' + \kappa\sqrt{\tau'(1+\tau')}}}, \quad (1)$$

where ξ_F is the dimensionless Fermi kinetic energy, and the following dimensionless transfer variables have been defined: $\lambda = \omega/2m_N$, $\kappa = q/2m_N$, $\tau = \kappa^2 - \lambda^2$. Primed variables contain an energy transfer shift, $\omega' = \omega - E_s$, which accounts (at least) for the binding energy of the ejected nucleon but is usually determined phenomenologically; for ^{12}C we use $E_s = 20$ MeV. The scaling variable considerably distorts the ω dependence, but it has the advantage of allowing us to easily locate the QE peak at $\Psi' = 0$, from which the peaks of the MEC responses are shifted. Over 100,000 terms are involved in the calculation, with subsequent seven-dimensional integrations, which make it a highly nontrivial computational procedure. In order to include these results in the neutrino generators used in the analysis of neutrino experiments, a parametrization of the MEC responses is essential to reduce the computational burden of performing the calculation for a large number of kinematic conditions (momentum and energy transfers).

The MEC response functions for $q \geq 400$ MeV/c exhibit a peak that decreases with q together with a tail that rises with Ψ' and q. In order to parametrize these functions, we applied an expression with two terms, the first one mainly fitting the peak of the response and the second fitting the tail at larger Ψ':

$$R_{T,\text{VV}}^{\text{MEC}}(\Psi') = \frac{2a_3 e^{-\frac{(\Psi'-a_4)^2}{a_5}}}{1 + e^{-\frac{(\Psi'-a_1)^2}{a_2}}} + \sum_{k=0}^{2} b_k(\Psi')^k. \quad (2)$$

In this expression, the parameters a_i, b_k are q dependent, and they are used to fit the original $R_{T,\text{VV}}^{\text{MEC}}$ responses shown in Fig. 1. We first fit each response for a given q to get the values of the a_i, b_k parameters for that specific q value, ensuring a smooth dependence on q for each of them. The q-dependent values of the fitting parameters are shown in Fig. 2. We then parametrize the q dependence of the parameters themselves using a polynomial in q. The response in Eq. (2) then becomes explicitly dependent on the momentum transfer $R_{T,\text{VV}}^{\text{MEC}}(\Psi', q)$ through the dependence in the parameters, $a_i(q)$, $b_k(q)$.

For the fitting of the responses above $q = 2000$ MeV/c, which show almost no peak but a tail-like shape, we keep only the second term in Eq. (2), namely, $a_3 = 0$; since these responses are very similar in the large-q region under consideration (up to 3500 MeV/c), we use the same parametrization for all of them, namely, $b_k(q > 2000) = b_k(q = 2000)$. In any case, as we can observe in Fig. 3, there are no significant MEC contributions for $q > 2000$ MeV/c and the same is true for large $\omega > 1000$ MeV. For the responses below $q = 300$ MeV/c, we use again a polynomial to fit the results,

$$R_{T,\text{VV}}^{\text{MEC}}(\Psi', q_{<300}) = \sum_{k=0}^{3} c_k(q)(\Psi')^k. \quad (3)$$
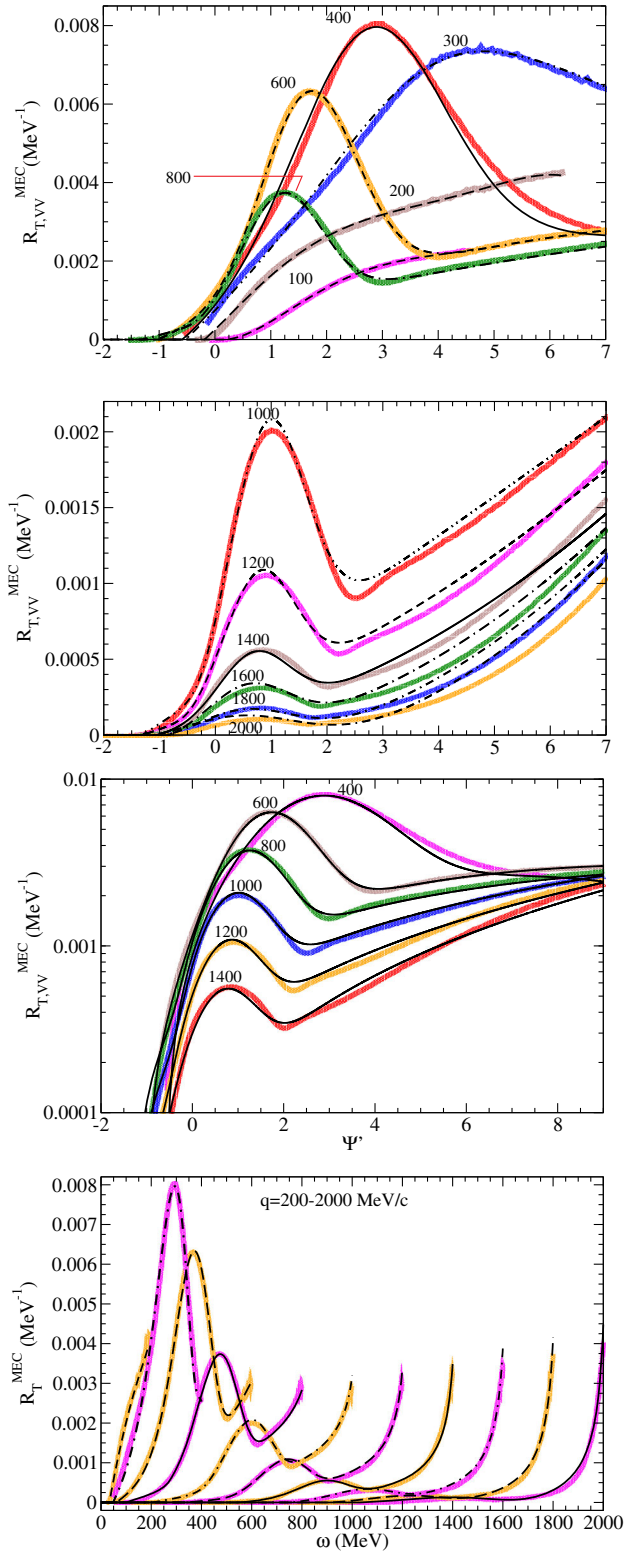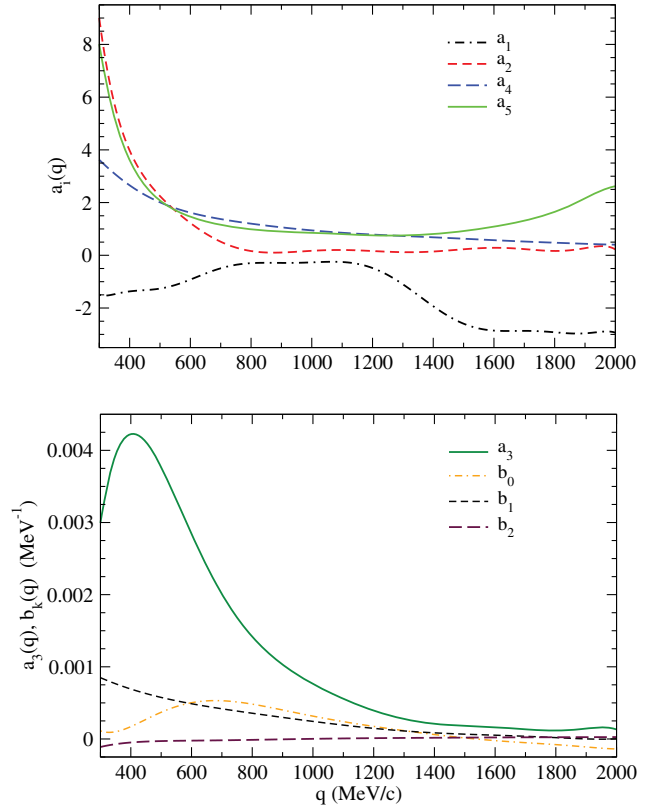
FIG. 2 (color online).   Dependence on q of the fitting parameters $\{a_i, b_k\}$.

The results of the above parametrization of the MEC responses are presented as a function of the scaling variable Ψ' in Fig. 1 where it is shown that it gives an excellent representation of the exact results in the full region of q and Ψ' explored.

As already mentioned, in previous work [10,27,28] a simple parametrization of the exact MEC calculation was used in order to evaluate the MiniBooNE (anti)neutrino cross sections. The present fit of the MEC responses improves the previous one in two respects: it uses data in a wider q range and includes the tail of the responses at high-Ψ' or -ω values. The previous parametrization was initially developed with electron scattering in mind, and, since (e, e') data are rarely available when $q \to \omega$, the high-ω region was ignored. Accordingly, the old parametrization missed the high-energy tails arising in the exact results and yielded lower peaks asymmetrically broadened towards higher-Ψ' values. In contrast, for CCQE reactions, one must integrate over a broad neutrino spectrum and, hence, potentially, the high-ω region may be relevant, and this motivated the reevaluation of the MEC contributions. In Fig. 1, we also show the $R_{T,VV}^{\mathrm{MEC}}$ results versus ω where it is noticed the negligible contribution below $q < 300$ MeV/c as well as the relevance of the tail in the response at $q > 800$ MeV/c. On the other hand, the tail of the MEC responses at high q ($q > 1000$ MeV/c), which appears at

FIG. 1 (color online). $R_{T,VV}^{\mathrm{MEC,param}}$ (MeV^{-1}) versus Ψ' (first three panels) and versus ω (bottom panel), where for the last one the curves are displayed from left to right in steps of $q = 200$ MeV/c. The parametrized responses are shown as black lines. Comparisons with Torino results (colored thick lines) are also displayed. Note that the y axis in the third panel is shown as a logarithmic scale.
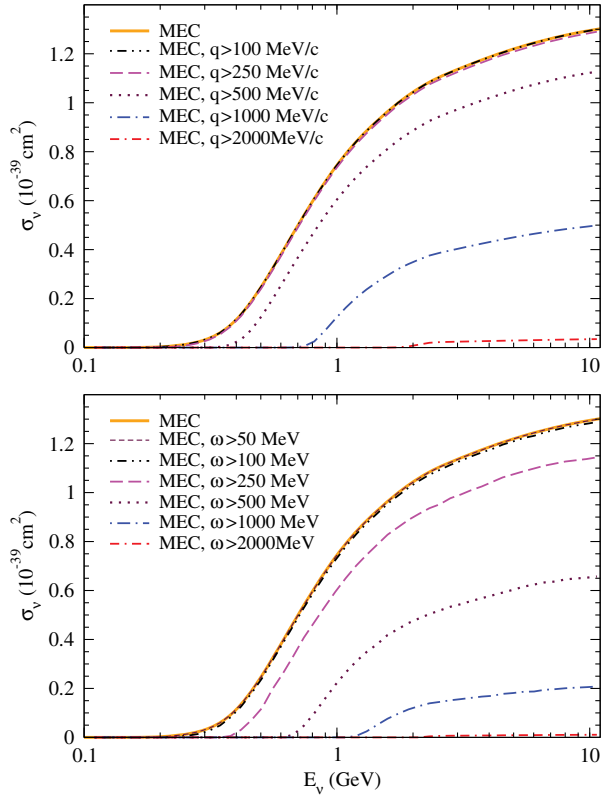
FIG. 3 (color online). Total MEC neutrino cross section per target nucleon evaluated excluding all contributions coming from transferred momentum (upper panel) and energy (lower panel) below some selected values, as indicated in the figure.

$\omega \gtrsim 1000$ MeV, does not contribute significantly to the cross section, as can be deduced from Fig. 3, and, in fact, the old and new parametrizations are observed to be very similar except at low neutrino energy where minor differences occur and at very high neutrino energy where the new parametrization yields somewhat larger contributions, as seen in Fig. 4.

In order to subtract some of the nucleonic and nuclear properties from the 2p-2h MEC parametrization, we can introduce a 2p-2h MEC isovector scaling function $f_{T,\mathrm{VV}}^{\mathrm{MEC}}$ defined analogously to the transverse scaling function coming from the transverse one-body response:

$$f_{T,\mathrm{VV}}^{\mathrm{MEC}}(\kappa,\lambda) = k_F \cdot \frac{R_{T,\mathrm{VV}}^{\mathrm{MEC}}(\kappa,\lambda)}{G_T(\kappa,\lambda)}, \qquad (4)$$

where the G_T factor depends on the momentum and energy transferred as well as on the isovector magnetic nucleon form factors, and k_F is the Fermi momentum of the nucleus. A detailed expression for G_T, including higher-order relativistic corrections, can be found in [39] and has been used in the calculation of $f_{T,\mathrm{VV}}^{\mathrm{MEC}}$ shown in Fig. 5. The remaining dependence on q of the scaling function seen in Fig. 5 is consistent with the violation of first-kind scaling
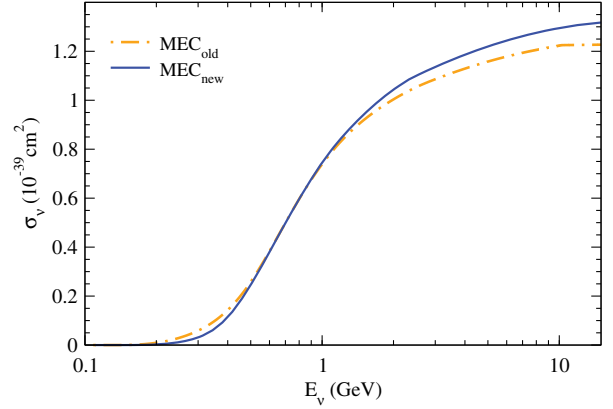

FIG. 4 (color online). Comparison between the total MEC cross section in the present and past parametrizations.

exhibited by the MECs [32]. The study of second-kind scaling violation related to the dependence on the nuclear species would require an in-depth study of the MEC contributions in other nuclei; some such studies were presented in [32].

For completeness, a comparison between our theoretical predictions and electron scattering data [40] at kinematics where MEC contributions are relevant, extending from the nonrelativistic to the highly inelastic regime, is also presented in Fig. 6. As shown, a model based solely on impulsive response function is not able to reproduce the (e, e') data. Contributions beyond the impulse approximation such as 2p-2h MECs could provide part of the missing strength in the transverse channel. Moreover, the addition of the impulsive inelastic contributions is shown to be essential to analyze the (e, e') data at high kinematics.

In general, the inelastic contributions can have a significant effect on the (e, e') cross section even in the QE regime, since the different domains can overlap. This agrees with the emerging pattern in Fig. 6 that suggests that the inclusion of inelastic processes—the contribution
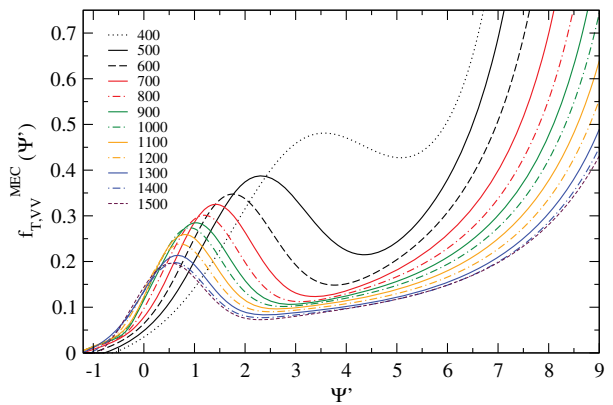

FIG. 5 (color online). Transverse 2p-2h MEC isovector scaling functions $f_{T,\mathrm{VV}}^{\mathrm{MEC}}$ versus the scaling variable Ψ' from $q = 400$ MeV/c to 1500 MeV/c.
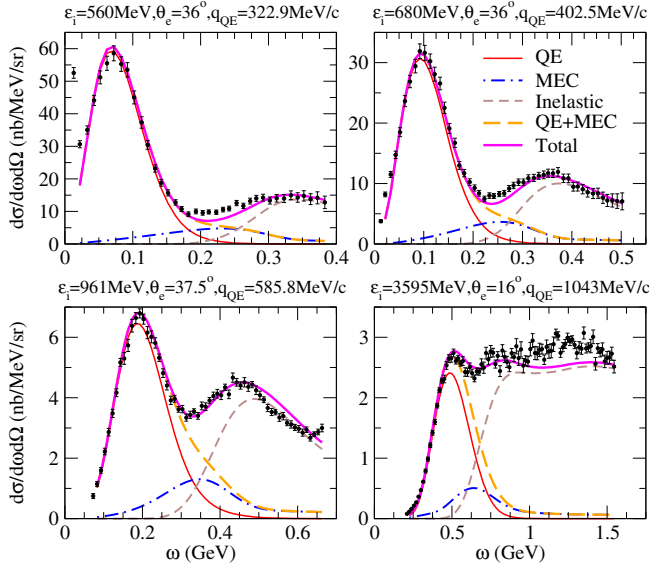
FIG. 6 (color online).   Comparison of inclusive ^{12}C(e, e') cross sections and predictions of the QE(SuSAv2), MEC, and inelastic (SuSAv2) models at different set values of the position of the QE peak (q_{QE}), incident electron energy (ε_i), and the scattering angle (θ_e). Data taken from [40].

of which clearly extends into the region dominated by quasielastic scattering—may lead to an enhancement of the theoretical results. The inelastic part of the cross section is dominated by the delta peak (mainly transverse) that contributes to the transverse response function. At low electron scattering angles, the longitudinal response function dominates the cross section, and the inelastic contribution is smaller. The opposite holds at large scattering angles, where the delta peak contribution is important. On the other hand, for increasing values of the transferred momentum, the peaks corresponding to the delta and QE domains become closer, and their overlap increases significantly. This general behavior is clearly shown by our predictions compared with the data. In those kinematical situations where inelastic processes are expected to be important, our results for the QE peak are clearly below the data. On the contrary, when the inelastic contributions are expected to be small, the QE theoretical predictions get closer to the data. It is important to point out that the description presented in this work corresponds to a semi-phenomenological model where the scaling function is fitted to the longitudinal (e, e') scattering data (and extended to the transverse response via the RMF theory). Thus, it does not encode the inelasticities that dominate the transverse response.

However, for completeness we also show in Fig. 6 some results for the inelastic contributions. As observed, the inclusion of the inelastic processes does not necessarily imply a "significant" enhancement of the cross section in the region close to the QE peak. In fact, at the particular kinematics considered in Fig. 6, the overlap between the

QE and inelastic regions is small, and, therefore, the agreement with the data in the QE region is not spoiled. However, more detailed results are needed before more definitive conclusions can be reached. In this sense, a new analysis of the inelastic channel based on the use of the recent SuSAv2 and MEC models will be presented in a forthcoming paper [11].

III. EVALUATION OF NEUTRINO CROSS SECTIONS

In this section, we evaluate the CCQE double-differential and total cross sections of (anti)neutrino scattering off ^{12}C using our latest SuSAv2 results and the new 2p-2h MEC parametrization. We compare the results with experimental data of MiniBooNE, NOMAD, and MINERνA.

As can be seen in Figs. 7 and 8, the inclusion of MEC results in an increase of the cross sections, yielding reasonable agreement with the MiniBooNE data for low angles, up to $\cos\theta_\mu \simeq 0.7$. At larger scattering angles, the disagreement with the experiment becomes more significant, and the vector-vector transverse MECs do not seem to be sufficient to account for the discrepancy. The same conclusion can be drawn by plotting the cross section versus the scattering angle (see Figs. 9 and 10) at fixed muon momentum; the inclusion of MECs improves the agreement with the data at low scattering angles, but some strength is missing at higher angles, especially for low muon momenta, as observed in [41].

The size of the MEC contribution to the cross section reported here—of the order of 10%—corresponds to the average value found within our particular RFG model. Our results show that processes involving MECs are responsible for a sizable enhancement of the response in the transverse channel. The extent to which this enhancement affects the cross section, however, strongly depends on the kinematics (see the discussion in the previous section).

We remark that axial-axial (AA) and vector-axial (VA) transverse MEC responses $R_{T,\mathrm{AA}}^{\mathrm{MEC}}$ and $R_{T',\mathrm{VA}}^{\mathrm{MEC}}$ are not considered in this work and could partially explain the discrepancy with the data. Furthermore, additional nuclear correlations could contribute to the 2p-2h excitations as the ones induced by MECs; however, since the longitudinal vector contributions come directly from experimental data and, hence, have all the correlations built in, such contributions would need to break zeroth-kind scaling, which has not been demonstrated. Note that extended RFG or RMF models with 2p-2h as well as 1p-1h correlations are actually required to preserve gauge invariance, but their inclusion would call for consistent treatments to avoid double counting.

When comparing our theoretical results with the MiniBooNE data, one can observe a better agreement for antineutrinos than for neutrinos (see Fig. 11). This is due to the fact that, in the neutrino case, the two missing MEC responses in our calculation are constructively
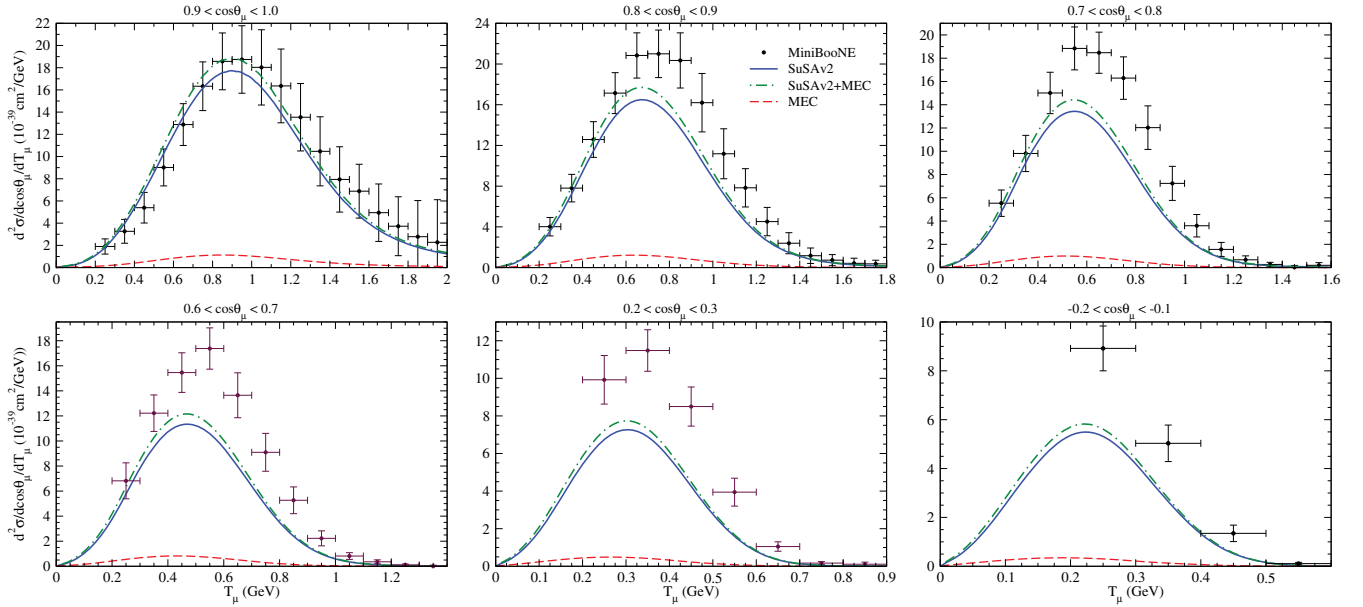
FIG. 7 (color online).   Flux-integrated double-differential cross section per target nucleon for the ν_μ CCQE process on ^{12}C displayed versus the μ^- kinetic energy T_μ for various bins of $\cos\theta_\mu$ obtained within the SuSAv2 and SuSAv2 + MECs approaches. MEC results are also shown. The data are from Ref. [2].
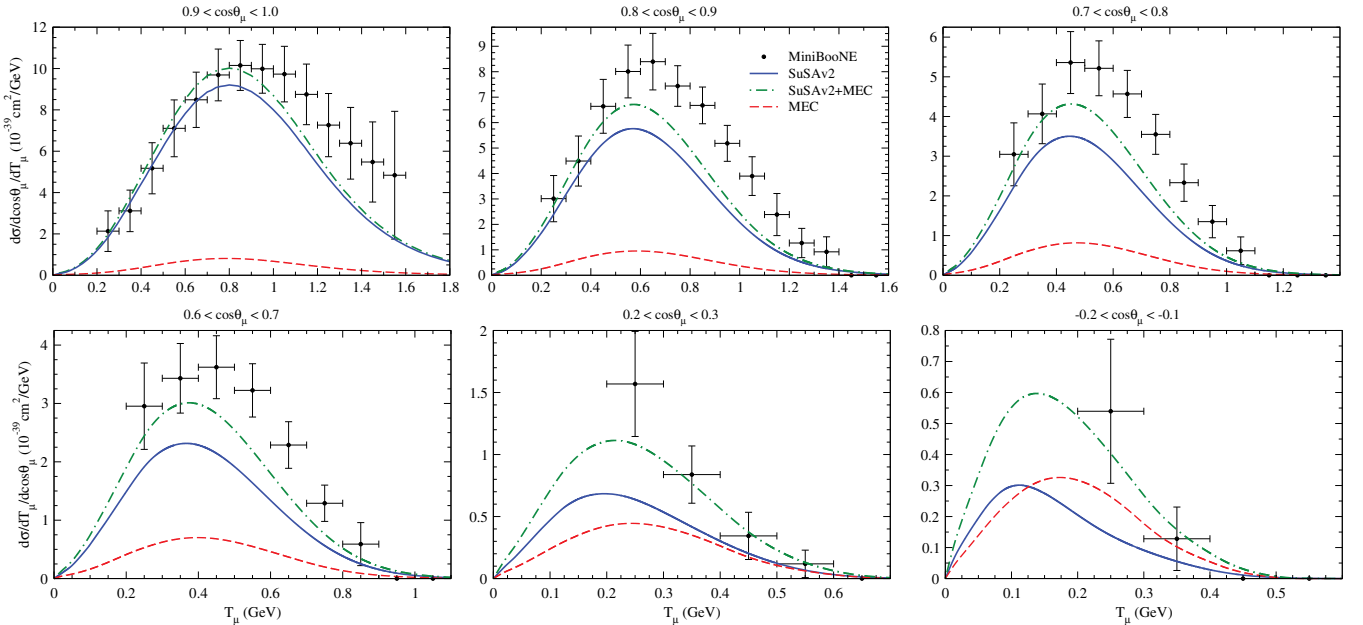

FIG. 8 (color online).   As for Fig. 7, but for $\bar{\nu}_\mu$ scattering versus μ^+ kinetic energy T_μ. The data are from Ref. [3].

combined, $R_{T,\text{AA}}^{\text{MEC}} + R_{T',\text{VA}}^{\text{MEC}}$, whereas they are destructively combined in the antineutrino case, $R_{T,\text{AA}}^{\text{MEC}} - R_{T',\text{VA}}^{\text{MEC}}$. In other words, we expect a larger strength missing in our calculation in the neutrino case than in the antineutrino case, whose origin possibly can be attributed to the missing MEC pieces. Furthermore, one can see in the total neutrino cross section (Fig. 11) that some strength is missing at intermediate energies, 0.4–1.5 GeV, which is the region

where the VA QE component is peaked (Fig. 12); an extra contribution in this channel via 2p-2h MECs would, thus, improve the agreement with MiniBooNE data. We can observe in Fig. 12 that below 1 GeV the SuSAv2 VA response is higher than the VV one and of the same order as the AA one. Other contributions to the VA response, apart from the QE one (SuSAv2), can be estimated as follows:
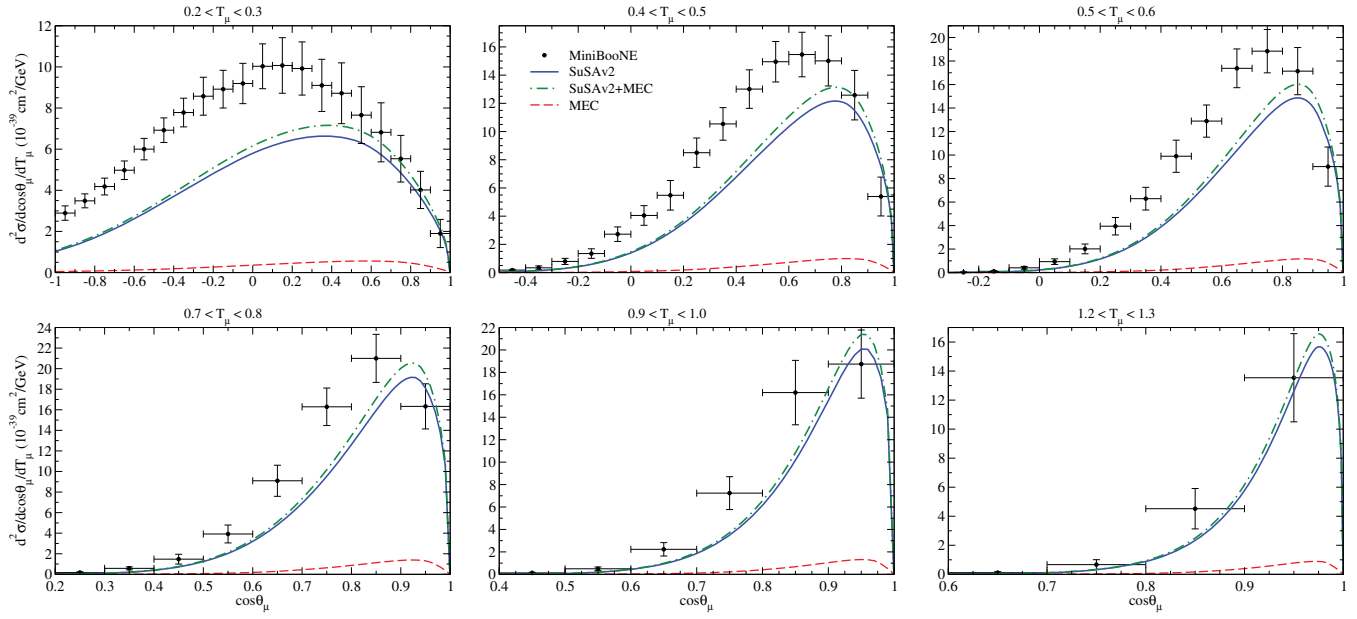
FIG. 9 (color online).   Flux-integrated double-differential cross section per target nucleon for the ν_μ CCQE process on ^{12}C displayed versus $\cos\theta_\mu$ for various bins of T_μ obtained within the SuSAv2 and SuSAv2 + MECs approaches. MEC results are also shown. The data are from Ref. [2].
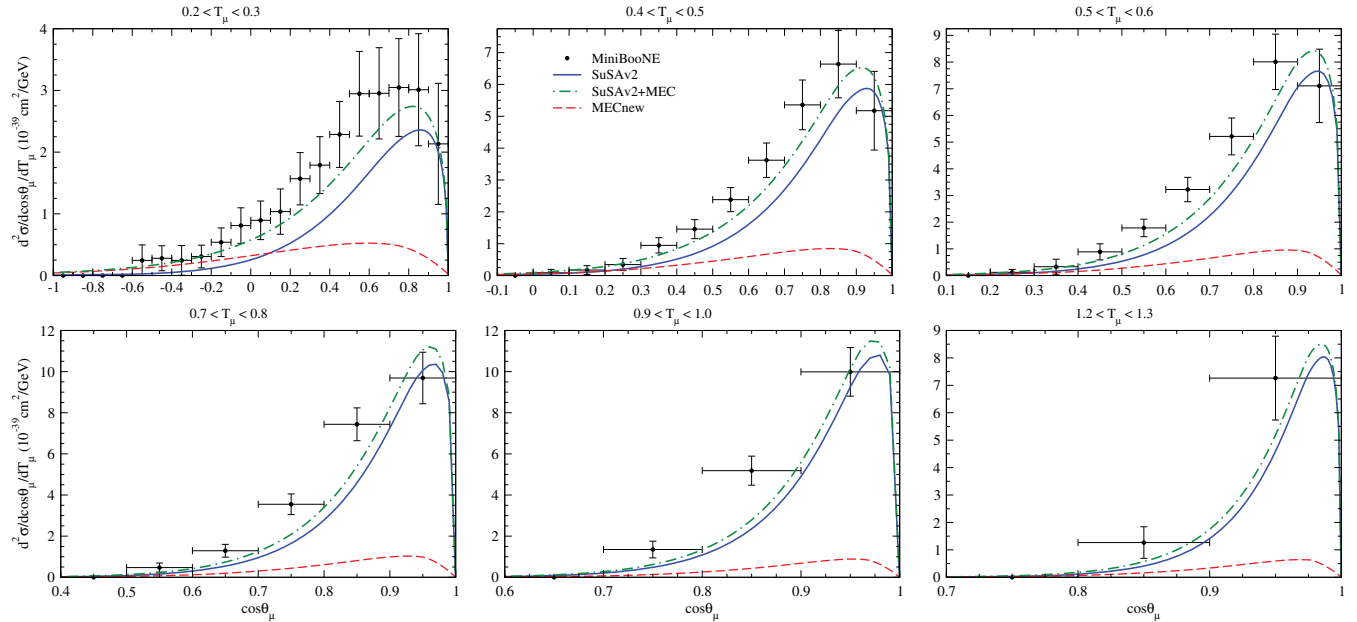

FIG. 10 (color online).   As for Fig. 9, but for $\bar{\nu}_\mu$ scattering versus $\cos\theta_\mu$. The data are from Ref. [3].

$$\left(\sigma_{\nu_\mu}\right)^{\text{other}}_{T',\text{VA}} \simeq \frac{\left(\sigma_{\nu_\mu} - \sigma_{\bar{\nu}_\mu}\right)_{\text{exp}}}{2} - \frac{\left(\sigma_{\nu_\mu} - \sigma_{\bar{\nu}_\mu}\right)_{\text{SuSAv2}}}{2}, \quad (5)$$

as long as one assumes no quenching of the axial current within the nuclear medium with respect to the vector current, as is the case in the superscaling approach. If one considers $\left(\sigma_{\nu_\mu}\right)^{\text{other}}_{T',\text{VA}}$ as mainly due to MECs, it is found

that a VA MEC response as large as the computed VV MEC response would be needed to reproduce the data. In Fig. 13 we show the experimental difference between neutrino and antineutrino cross sections $\left(\sigma_{\nu_\mu} - \sigma_{\bar{\nu}_\mu}\right)_{\text{exp}}$ from MiniBooNE, together with the corresponding theoretical prediction from SuSAv2, which is approximately equal to $2\left(\sigma_{\nu_\mu}\right)^{\text{SuSAv2}}_{T'\text{VA}}$. The theoretical result from SuSAv2 with VV
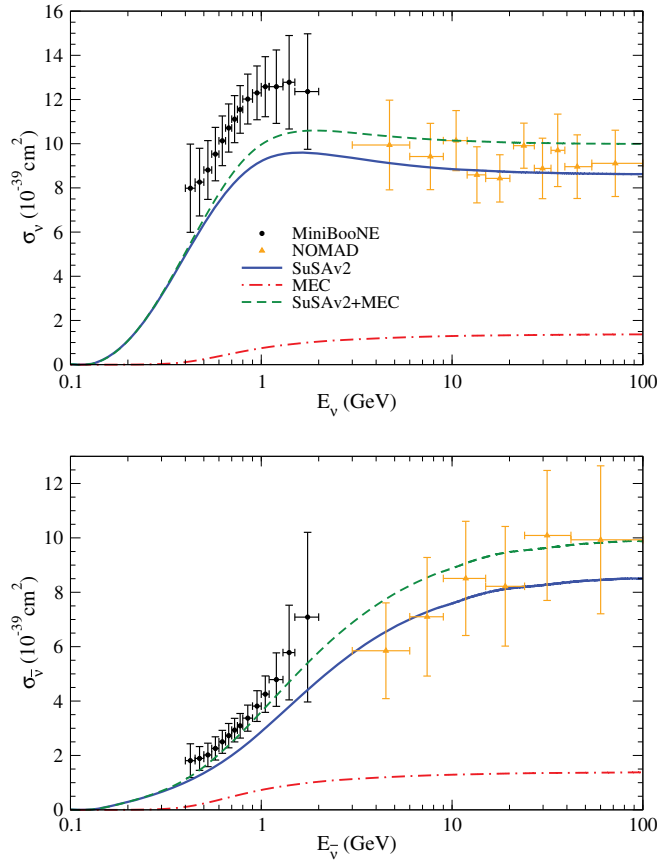
FIG. 11 (color online). CCQE ν_μ cross section per nucleon displayed versus neutrino energy E_ν and evaluated using the SuSAv2 and the SuSAv2 + MECs approaches (top panel). CCQE $\bar{\nu}_\mu$ cross section is also shown (bottom panel). Results are compared with the MiniBooNE [2,3] and NOMAD [7] experimental data. Also presented for reference are the results for the MEC contributions.
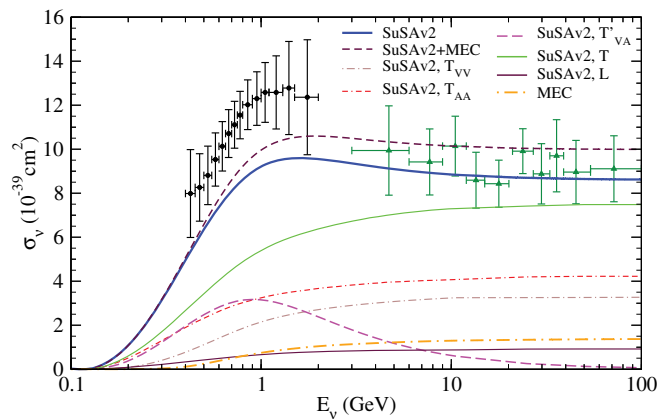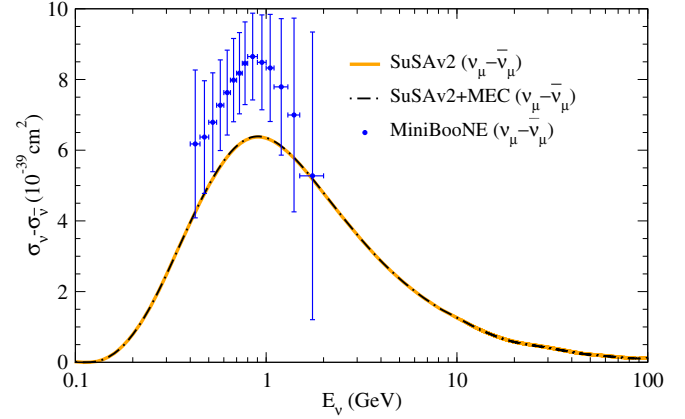

FIG. 12 (color online). Separation into components of the CCQE ν_μ cross section per nucleon displayed versus neutrino energy E_ν within the SuSAv2 approach. The MECs and SuSAv2 + MECs curves are shown. The MiniBooNE [2] and NOMAD [7] data are also shown for reference.

FIG. 13 (color online). Experimental difference between neutrino and antineutrino cross sections $(\sigma_{\nu_\mu} - \sigma_{\bar{\nu}_\mu})$ from MiniBooNE, together with the corresponding theoretical prediction from SuSAv2 + MECs, whose difference with the SuSAv2 prediction is negligible.

MEC contributions is also shown in the figure but is almost indistinguishable from the SuSAv2 result due to the VV character of the MECs used. Apart from the opposite sign in the VA response, some minor differences between neutrino and antineutrino cross sections arise from the different Coulomb distortions of the emitted lepton [12] and the final nuclei involved in the CC neutrino (nitrogen) and antineutrino (boron) scattering processes.

It can be seen that an extra contribution to the VA response from MECs would improve the agreement with the data for the difference between neutrino and antineutrino total cross sections of MiniBooNE, as was noted above for just the neutrino case. In the same way, one could deduce the suitability of extra AA and VA contributions via MECs in the double-differential MiniBooNE cross section by analyzing Figs. 14 and 15. At NOMAD kinematics, Fig. 11, we observe a good agreement of the SuSAv2 + MECs results, partly due to the negligible contribution of the VA response, whose MEC part is missing in our calculation, in such high-energy processes (E_ν between 5 and 100 GeV). From Fig. 12 one sees that the VA interference becomes very small for $E_\nu > 5$ GeV; this arises because the scattering at NOMAD kinematics is very forward peaked, and as $\theta_\mu \to 0$, the factor $v_{T'} \to 0$ (see Ref. [39]). This is also in agreement with some previous QE results [42].

While work is in progress to compute the weak responses with all the V and A contributions, we have found that assuming the transverse vector 2p-2h MEC scaling function, $f_{T,VV}^{MEC}$, to equal the axial-axial ($f_{T,AA}^{MEC}$) and vector-axial ($f_{T',VA}^{MEC}$) ones—as done, for instance, in [8]—a final result in agreement with MiniBooNE data is found. On the contrary, the calculation slightly overestimates NOMAD data. However, such results cannot be fully justified until a proper 2p-2h MEC calculation for the axial-axial and
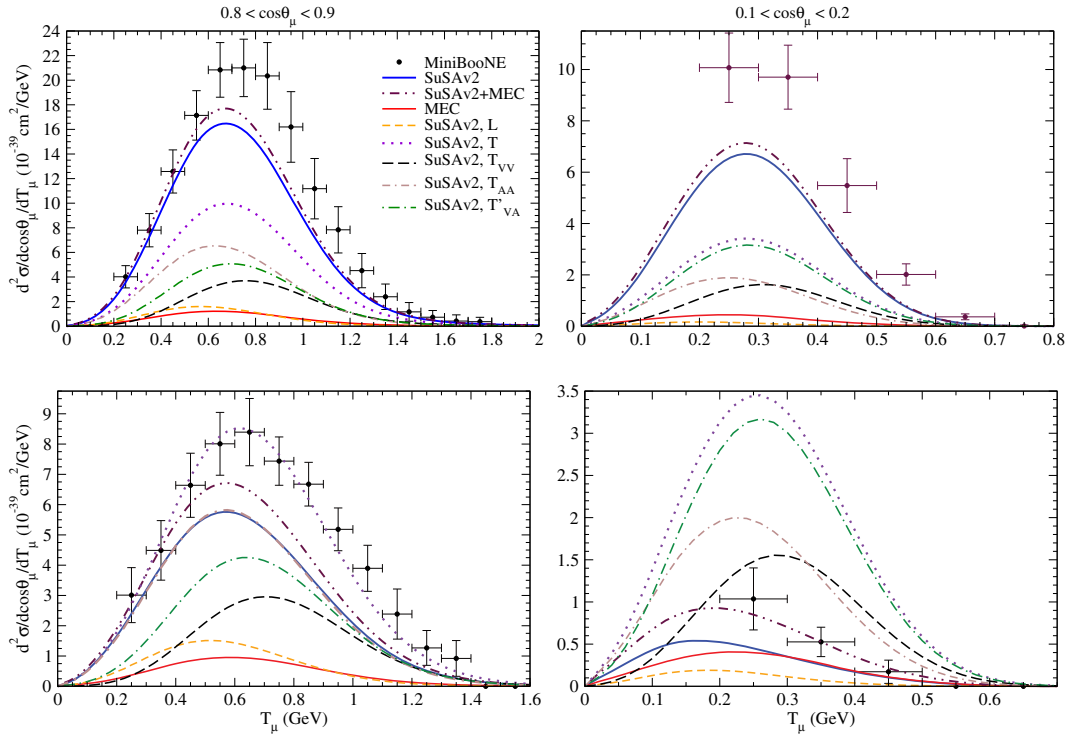
FIG. 14 (color online).   Separation into components of the MiniBooNE CCQE ν_μ (top panel) and $\bar{\nu}_\mu$ (bottom panel) double-differential cross section per nucleon displayed versus T_μ for various bins of $\cos\theta_\mu$ within the SuSAv2 approach. The MECs and SuSAv2 + MECs curves are shown. The MiniBooNE [2,3] data are also shown for reference.
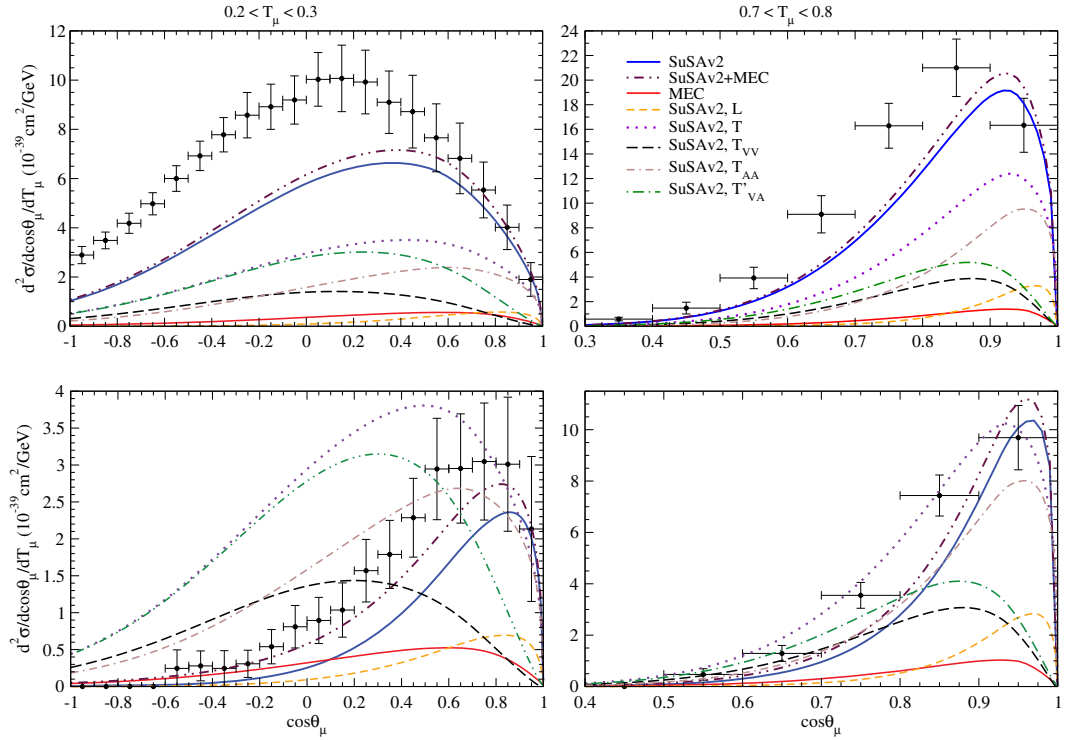

FIG. 15 (color online).   Separation into components of the MiniBooNE CCQE ν_μ (top panel) and $\bar{\nu}_\mu$ (bottom panel) double-differential cross section per nucleon displayed versus $\cos\theta_\mu$ for various bins of T_μ within the SuSAv2 approach. The MECs and SuSAv2 + MECs curves are shown. The MiniBooNE [2,3] data are also shown for reference.
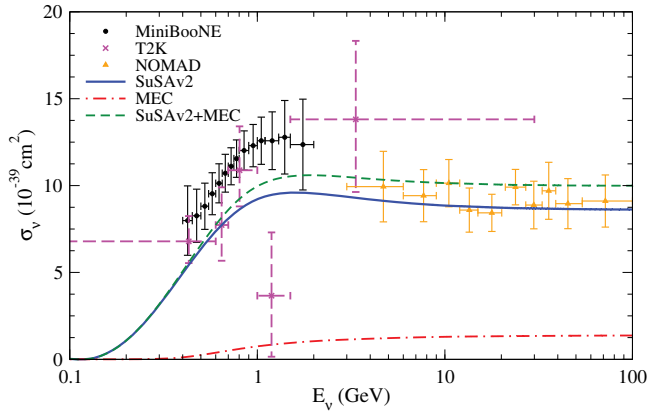
FIG. 16 (color online). CCQE ν_μ cross section per nucleon displayed versus neutrino energy E_ν and evaluated using the SuSAv2 and the SuSAv2 + MECs approaches. Results are compared with the MiniBooNE [2,3], NOMAD [7], and T2K [43] experimental data. Also presented for reference are the results for the MEC contributions.

vector-axial responses is completed. Moreover, one should take note of the different ways to analyze the QE-like events in MiniBooNE and NOMAD, where in the latter [7], the combination of one-track and two-track samples in the
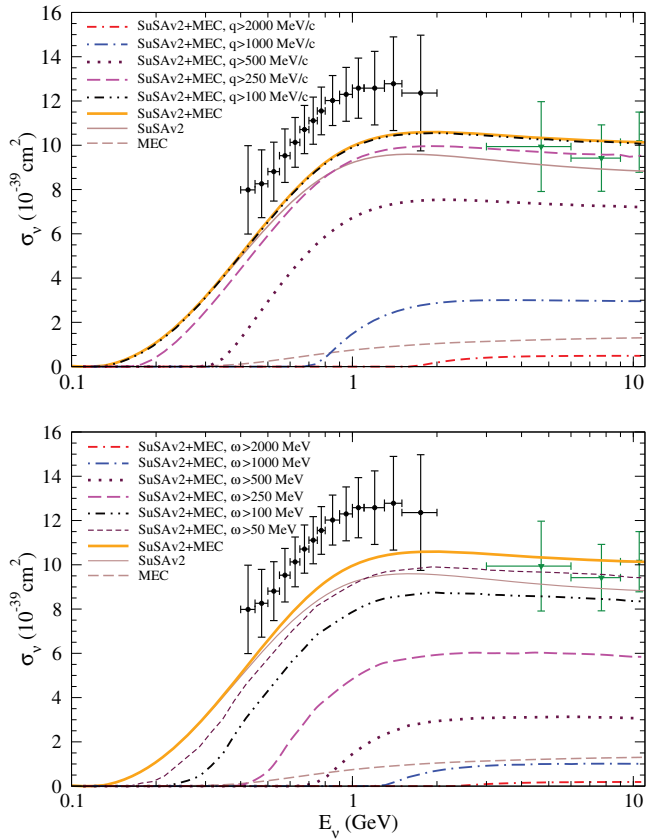

FIG. 17 (color online). As for Fig. 3, but for the SuSAv2 + MECs CCQE cross section. The MiniBooNE [2] and NOMAD [7] data are also shown for reference.
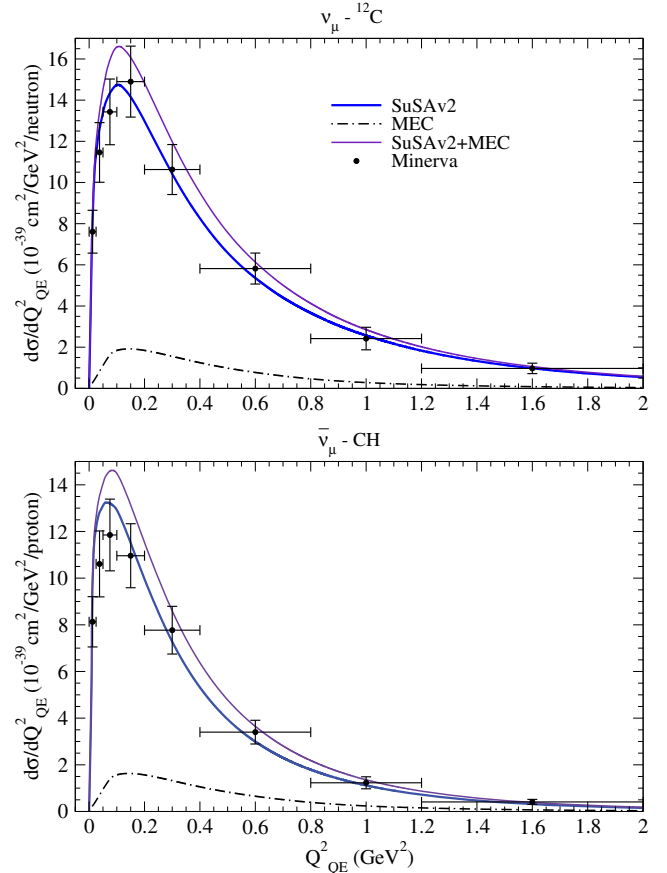

FIG. 18 (color online). Flux-folded CCQE $\nu_\mu - {}^{12}\text{C}$ (upper panel) and $\bar{\nu}_\mu - \text{CH}$ (lower panel) scattering cross section per target nucleon as a function of Q^2_{QE} and evaluated in the SuSAv2 and SuSAv2 + MECs models. MINERνA data are from [4,5].

case of $\nu_\mu n \rightarrow \nu^- p$ can help to reduce some uncertainties as well as some contributions beyond the impulse approximation, such as from MECs or correlations that eject two nucleons. For completeness, we also show in Fig. 16 recent results from the T2K Collaboration [43]. One should notice that, as they state, "There is consistency between the experiments within the current statistical and systematic uncertainties."

Moreover, an analysis of the relevant kinematic regions in the SuSAv2 + MECs cross section is shown in Fig. 17, where it is observed that the main contribution to the total cross section comes from $\omega < 1000$ MeV and $q \lesssim 1000$ MeV/c, whereas the region of $\omega < 50$ MeV and $q < 250$ MeV/c is not too significant for the cross section (less than 10%). This is in accordance with some previous works [42,44]. The same conclusion can be drawn by analyzing the different kinematics in the total MEC cross section (Fig. 3), where the low kinematic region ($\omega < 50$ MeV, $q < 250$ MeV/c) is even less important (<2%).

At MINERνA kinematics, a good agreement arises for the purely QE SuSAv2 model with the $d\sigma/dQ^2_{\text{QE}}$ data
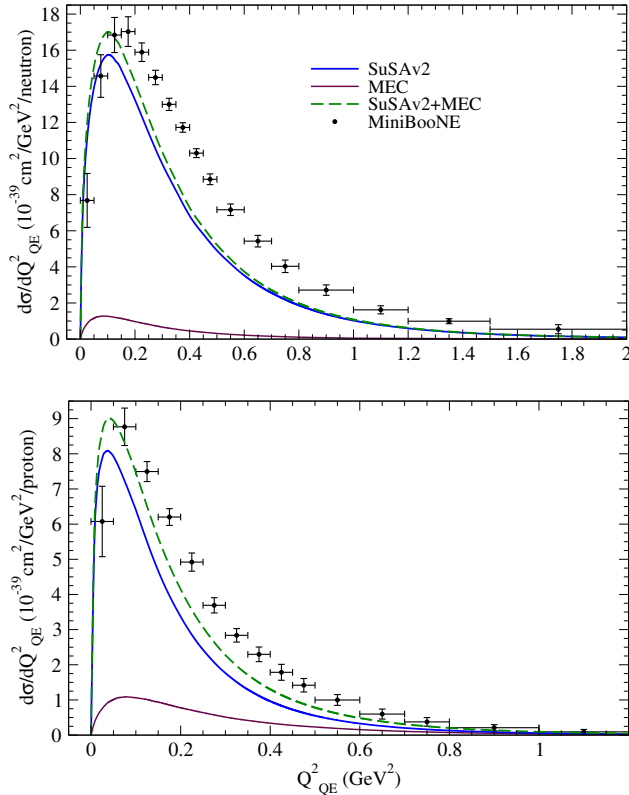
FIG. 19 (color online). Flux-folded CCQE $\nu_\mu - {}^{12}C$ (upper panel) and $\bar{\nu}_\mu - {}^{12}C$ (lower panel) scattering cross section per target nucleon as a function of Q^2_{QE} and evaluated in the SuSAv2 and SuSAv2 + MECs models. MiniBooNE data are from [2,3].

without additional assumptions, Fig. 18, as observed in [44] for other impulse-approximation-based models. An overestimation of the data shows up at low Q^2_{QE} when adding 2p-2h MEC contributions. On the contrary, this effect is not observed in the same differential cross sections of MiniBooNE, Fig. 19, which is an example of the discrepancies between the two experiments and their different ways to proceed in the data analysis.

IV. CONCLUSIONS

We have obtained CCQE neutrino-${}^{12}C$ cross sections using the SuSAv2 scaling procedure and a new parametrization of 2p-2h vector-vector transverse MECs. Both ingredients are based on relativistic models (RMF, RFG, RPWIA), as demanded by the kinematics of present and future high-energy neutrino experiments, where traditional nonrelativistic models are questionable. We do not include in this work axial-axial and vector-axial MEC contributions needed for the analysis of neutrino scattering processes, or correlation diagrams—the calculation of the

axial MEC contributions is currently being considered using [25,26].

Any model aimed at providing a useful and reliable tool to be employed in the analysis of experimental studies of neutrino oscillations needs their limits of applicability to be completely understood. This has been the case in our present study where the limits of the approach have been stated clearly and discussed at length. Various models rely on different assumptions: nonrelativistic expansions, factorization approach, mean field, etc., that restrict their reliability. However, in the absence of a "fully unlimited" description of the reaction mechanism, the use of consistent, even limited, theoretical predictions to be contrasted with the data allows one to get insight into the physics underlying neutrino experiments. Hence, in spite of the limitations mentioned above, our present model provides results that are in accordance with (e, e') data in the region around the QE peak. This is of great importance, and it gives us confidence in the consistency and validity of our calculations in order to analyze lepton-nucleus scattering.

By comparing these results with the experimental data of the MiniBooNE, NOMAD, and MINERνA collaborations, we have shown that 2p-2h MECs play an important role in CCQE neutrino scattering and may help to resolve the controversy between theory and experiment. The main merit of the parametrization provided here is that it translates a sophisticated and computationally demanding microscopic calculation of MECs into a smooth parametrization which is dependent on the values of the transfer variables of the process. The economy of this MEC parametrization together with the one inherent in a scaling approach might be of interest to Monte Carlo neutrino event simulations used in the analysis of experiments.

ACKNOWLEDGMENTS

[1] Note that, as is common in discussions of electron scattering, we define QE to mean the part of the cross section arising from nucleon knockout via one-body operators. This is to be distinguished from contributions that arise through the action of two-body operators such as the MEC effects discussed in the present work. The latter can eject single nucleons or two nucleons (or in fact no nucleons at all, as in elastic scattering). In contrast, what is referred to as "quasielastic" in the neutrino community really means the "no-pion cross section" and that should contain both one- and two-body current operators, but should have no pions produced in the final state. Indeed, one common concern is how much model dependence occurs in defining this no-pion cross section, since corrections must be made for events where a pion is actually produced, but is absorbed before being detected and hence mistaken as a "quasielastic" event.

[2] A. A. Aguilar-Arevalo *et al.* (MiniBooNE Collaboration), Phys. Rev. D **81**, 092005 (2010).

[3] A. A. Aguilar-Arevalo *et al.* (MiniBooNE Collaboration), Phys. Rev. D **88**, 032001 (2013).

[4] L. Fields *et al.* (MINERνA Collaboration), Phys. Rev. Lett. **111**, 022501 (2013).

[5] G. A. Fiorentini *et al.* (MINERνA Collaboration), Phys. Rev. Lett. **111**, 022502 (2013).

[6] P. Adamson *et al.*, Phys. Rev. D **91**, 012005 (2015).

[7] V. Lyubushkin *et al.* (NOMAD Collaboration), Eur. Phys. J. C **63**, 355 (2009).

[8] M. Martini, M. Ericson, G. Chanfray, and J. Marteau, Phys. Rev. C **80**, 065501 (2009).

[9] J. Nieves, I. Ruiz-Simo, and M. J. Vicente-Vacas, Phys. Rev. C **83**, 045501 (2011).

[10] J. E. Amaro, M. B. Barbaro, J. A. Caballero, T. W. Donnelly, and J. M. Udías, Phys. Rev. D **84**, 033004 (2011).

[11] In devising both the SuSA and SuSAv2 models comparisons have been made with existing ^{12}C QE inclusive electron scattering data. The detailed results of those studies will be presented in a future paper (to be published).

[12] J. E. Amaro, M. B. Barbaro, J. A. Caballero, T. W. Donnelly, A. Molinari, and I. Sick, Phys. Rev. C **71**, 015501 (2005).

[13] D. B. Day, J. S. McCarthy, T. W. Donnelly, and I. Sick, Annu. Rev. Nucl. Part. Sci. **40**, 357 (1990).

[14] T. W. Donnelly and I. Sick, Phys. Rev. Lett. **82**, 3212 (1999).

[15] T. W. Donnelly and I. Sick, Phys. Rev. C **60**, 065502 (1999).

[16] R. González-Jiménez, G. D. Megias, M. B. Barbaro, J. A. Caballero, and T. W. Donnelly, Phys. Rev. C **90**, 035501 (2014).

[17] J. A. Caballero, J. E. Amaro, M. B. Barbaro, T. W. Donnelly, C. Maieron, and J. M. Udías, Phys. Rev. Lett. **95**, 252502 (2005).

[18] J. A. Caballero, Phys. Rev. C **74**, 015502 (2006).

[19] J. A. Caballero, J. E. Amaro, M. B. Barbaro, T. W. Donnelly, and J. M. Udías, Phys. Lett. B **653**, 366 (2007).

[20] C. Maieron, J. E. Amaro, M. B. Barbaro, J. A. Caballero, T. W. Donnelly, and C. F. Williamson, Phys. Rev. C **80**, 035504 (2009).

[21] J. E. Amaro, M. B. Barbaro, J. A. Caballero, T. W. Donnelly, and A. Molinari, Phys. Rep. **368**, 317 (2002).

[22] J. E. Amaro, M. B. Barbaro, J. A. Caballero, T. W. Donnelly, and A. Molinari, Nucl. Phys. **A723**, 181 (2003).

[23] W. Alberico, T. W. Donnelly, and A. Molinari, Nucl. Phys. **A512**, 541 (1990).

[24] J. E. Amaro, M. B. Barbaro, J. A. Caballero, T. W. Donnelly, C. Maieron, and J. M. Udias, Phys. Rev. C **81**, 014606 (2010).

[25] I. Ruiz-Simo, C. Albertus, J. E. Amaro, M. B. Barbaro, J. A. Caballero, and T. W. Donnelly, Phys. Rev. D **90**, 033012 (2014).

[26] I. Ruiz-Simo, C. Albertus, J. E. Amaro, M. B. Barbaro, J. A. Caballero, and T. W. Donnelly, Phys. Rev. D **90**, 053010 (2014).

[27] J. E. Amaro, M. B. Barbaro, J. A. Caballero, T. W. Donnelly, and C. F. Williamson, Phys. Lett. B **696**, 151 (2011).

[28] J. E. Amaro, M. B. Barbaro, J. A. Caballero, and T. W. Donnelly, Phys. Rev. Lett. **108**, 152501 (2012).

[29] A. D. Pace, M. Nardi, W. M. Alberico, T. W. Donnelly, and A. Molinari, Nucl. Phys. **A726**, 303 (2003).

[30] O. Benhar, A. Lovato, and N. Rocco, arXiv:1312.1210.

[31] J. E. Amaro, C. Maieron, M. B. Barbaro, J. A. Caballero, and T. W. Donnelly, Phys. Rev. C **82**, 044601 (2010).

[32] A. D. Pace, M. Nardi, W. M. Alberico, T. W. Donnelly, and A. Molinari, Nucl. Phys. **A741**, 249 (2004).

[33] J. E. Amaro, G. Co, E. M. V. Fasanelli, and A. M. Lallena, Phys. Lett. B **277**, 249 (1992).

[34] J. E. Amaro, G. Co, and A. M. Lallena, Nucl. Phys. **A578**, 365 (1994).

[35] J. W. V. Orden and T. W. Donnelly, Ann. Phys. (N.Y.) **131**, 451 (1981).

[36] W. M. Alberico, M. Ericson, and A. Molinari, Ann. Phys. (N.Y.) **154**, 356 (1984).

[37] M. J. Dekker, P. J. Brussaard, and J. A. Tjon, Phys. Rev. C **49**, 2650 (1994).

[38] A. Gil, J. Nieves, and E. Oset, Nucl. Phys. **A627**, 543 (1997).

[39] J. E. Amaro, M. B. Barbaro, J. A. Caballero, T. W. Donnelly, and C. Maieron, Phys. Rev. C **71**, 065501 (2005).

[40] O. Benhar, D. Day, and I. Sick, Rev. Mod. Phys. **80**, 189 (2008).

[41] M. V. Ivanov, A. N. Antonov, J. A. Caballero, G. D. Megias, M. B. Barbaro, E. Moya de Guerra, and J. M. Udías, Phys. Rev. C **89**, 014607 (2014).

[42] G. D. Megias, J. E. Amaro, M. B. Barbaro, J. A. Caballero, and T. W. Donnelly, Phys. Lett. B **725**, 170 (2013).

[43] K. Abe *et al.* (T2K Collaboration), arXiv:1411.6264.

[44] G. D. Megias, M. V. Ivanov, R. González-Jiménez, J. A. Caballero, M. B. Barbaro, T. W. Donnelly, and J. M. Udías, Phys. Rev. D **89**, 093002 (2014).